Solar Energy 159 (2018) 940–946

Contents lists available at ScienceDirect

Solar Energy

journal homepage: www.elsevier.com/locate/solener

Structural and chemical evolution of the CdS:O window layer during individual CdTe solar cell processing steps

A. Abbas[a], D.M. Meysing[b,c], M.O. Reese[c], T.M. Barnes[c], J.M. Walls[a], C.A. Wolden[b,*]

[a] Loughborough University, Loughborough, Leicestershire LE11 3TU, United Kingdom
[b] Colorado School of Mines, Golden, CO 80401, USA
[c] National Renewable Energy Laboratory, Golden, CO 80401, USA

ARTICLE INFO

Keywords:
Oxygenated CdS
CdTe solar cells
Cadmium sulfate
TEM

ABSTRACT

Oxygenated cadmium sulfide (CdS:O) is often used as the *n*-type window layer in high-performance CdTe heterojunction solar cells. The as-deposited layer prepared by reactive sputtering is XRD amorphous, with a bulk composition of $CdS_{0.8}O_{1.2}$. Recently it was shown that this layer undergoes significant transformation during device fabrication, but the roles of the individual high temperature processing steps was unclear. In this work high resolution transmission electron microscopy coupled to elemental analysis was used to understand the evolution of the heterojunction region through the individual high temperature fabrication steps of CdTe deposition, $CdCl_2$ activation, and back contact activation. It is found that during CdTe deposition by close spaced sublimation at 600 °C the CdS:O film undergoes recrystallization, accompanied by a significant (~30%) reduction in thickness. It is observed that oxygen segregates during this step, forming a bi-layer morphology consisting of nanocrystalline CdS adjacent to the tin oxide contact and an oxygen-rich layer adjacent to the CdTe absorber. This bilayer structure is then lost during the 400 °C $CdCl_2$ treatment where the film transforms into a heterogeneous structure with cadmium sulfate clusters distributed randomly throughout the window layer. The thickness of window layer remains essentially unchanged after $CdCl_2$ treatment, but a ~25 nm graded interfacial layer between CdTe and the window region is formed. Finally, the rapid thermal processing step used to activate the back contact was found to have a negligible impact on the structure or composition of the heterojunction region.

1. Introduction

Cadmium telluride (CdTe) has emerged as the leading thin-film photovoltaic (PV) technology and is poised to reach grid parity soon with record device efficiency currently at 22.1% (Green et al., 2017). Cadmium sulfide (CdS) is the most commonly used window layer in CdTe photovoltaic devices (McCandless and Sites, 2003). This layer provides a receptive surface for CdTe nucleation and growth, and forms a high quality heterojunction with the absorber. However, light absorbed by CdS generates negligible photocurrent, so quantum efficiency (QE) is attenuated at wavelengths below the CdS band gap (520 nm) (Sites, 2003). Photocurrent losses can be decreased by reducing thickness, but only to a degree. As the CdS thickness is reduced efficiency can decline due to deterioration in both open circuit voltage (V_{oc}) and fill factor (FF) (Nakamura et al., 2003; Hädrich et al., 2009). To circumvent this trade off there has been intensive work to develop alternative window layers (Kartopu et al., 2014), with one of the most successful being oxygenated cadmium sulfide (CdS:O) which was originally introduced by Wu and co-workers (Wu et al., 2002).

CdS:O is typically deposited by reactive sputtering of CdS at low temperature using a dilute O_2/Ar mixture (Kephart et al., 2012, 2015; Paudel and Yan, 2013; Paudel et al., 2014; Klein, 2015; Meysing et al., 2015a). As the fraction of oxygen in the sputter ambient increases film crystallinity is reduced and the optical band gap increases. Performance gradually improves with increasing optical band gap, reaches a maximum, and then drops dramatically (Paudel and Yan, 2013; Kephart et al., 2015; Meysing et al., 2015b). The oxygen content in as-deposited CdS:O can reach 45 at.% via sulfate group ($CdSO_4$) incorporation (Soo et al., 2006; Kephart et al., 2015; Klein, 2015; Meysing et al., 2015b). Efficiency gains are achieved primarily through increases in J_{sc} due to improvements in short-wavelength quantum efficiency without compromising V_{oc} or FF. The successful use of CdS:O requires careful optimization of sputter conditions, but high performance devices with power conversion efficiencies ranging from 15.2 to 16.4% have been achieved independently by several groups (Wu et al., 2004; Paudel and Yan, 2013; Kephart et al., 2015; Mahabaduge et al., 2015; Turck et al.,

* Corresponding author.
E-mail address: cwolden@mines.edu (C.A. Wolden).

https://doi.org/10.1016/j.solener.2017.11.051
Received 29 June 2017; Received in revised form 10 November 2017; Accepted 20 November 2017

Table 1
Representative device parameters for the four processing combinations.

#	Processing	J_{sc} (mA/cm^2)	V_{OC} (mV)	FF (%)	η (%)
1	No $CdCl_2$ No RTP	4	450	25	0.45
2	$CdCl_2$ No RTP	7	463	47	1.53
3	No $CdCl_2$ RTP	4.7	480	46	1.03
4	$CdCl_2$ RTP	25	853	75	16.0

2016).

In the conventional superstrate architecture, the CdTe absorber is deposited directly on CdS:O at high temperature (500–600 °C) by close spaced sublimation (CSS) or vapor transport deposition (VTD), which is followed by an annealing step in the presence of $CdCl_2$ at T ~ 400 °C. Lastly, the back contact is either applied at elevated temperature or subjected to a thermal activation step (200–400 °C). These high-temperature, reactive environments likely cause significant changes to the underlying CdS:O material (Paudel et al., 2014; Kephart et al., 2015). For example, in the case of the conventional CdS/CdTe solar cells it has been demonstrated that there is considerable interdiffusion, with sulfur substituting into the CdTe zinc blende structure ($CdTe_{1-x}S_x$) and conversely Te substituting into the CdS wurtzite structure (CdS_yTe_{1-y}) (McCandless et al., 2001). Lane and co-workers (Lane et al., 2000) performed a detailed microstructural analysis and found that the composition on both sides of the interface reach their respective equilibrium alloy composition based on the process temperature. A sulfur gradient then extends into the CdTe absorber. In the case of the thin window layer there may be a Te gradient present or the layer may be fully transformed into the equilibrium alloy composition, depending on temperature and duration of processing (Lane et al., 2000). This interdiffusion process is now quite well understood for conventional CdS/CdTe heterojunctions, but a similar examination of CdS:O/CdTe-based devices has not been reported.

Direct characterization of the window region with high fidelity in completed devices is extraordinarily difficult because this ~100 nm layer is sandwiched between a TCO-coated glass superstrate and several microns of the CdTe absorber. Using two approaches to isolate the window layer in completed devices (Meysing et al., 2015a) and a suite of complementary characterization we were able to reveal the significant changes that occur to the CdS:O window layer during device processing (Meysing et al., 2016). It was shown that CdS:O is transformed into a nanocrystalline $CdS_{1-y}Te_y$ alloy whose composition approaches solubility limits (y ~ 0.1). A substantial fraction of oxygen remains after device processing, segregated into cadmium sulfate ($CdSO_4$) clusters distributed throughout the window layer. The previous studies revealed the cumulative transformation that occurs during device fabrication, but the impact of individual processing steps remains unknown. After CdS:O deposition there are three high temperature fabrication steps: CdTe deposition, $CdCl_2$ treatment, and back contact activation. In this paper we use high resolution transmission electron microscopy (HR-TEM) and chemical mapping to assess the changes induced to the structure and composition of the window layer by these individual processes. It is shown that the first two steps both induce substantial changes, whereas the latter does not.

2. Experimental

Devices in this work were fabricated in the superstrate configuration using Corning 7059 glass coated with a fluorinated and intrinsic tin oxide bilayer using chemical vapor deposition. In previous studies, it was found that the 2.8 eV CdS:O produced optimal device performance using our process (Meysing et al., 2015b). Films were deposited at ambient temperature by rf magnetron sputtering using a stoichiometric CdS target (Materion, 99.99% purity) in a Unifilm PVD-300 sputtering system. A 4% O_2/Ar mixture was used to produce the 2.8 eV CdS:O, and the film thickness was fixed at 100 nm as confirmed by ellipsometry. Approximately 4 μm of CdTe was deposited on CdS:O layers using CSS. The source and substrate temperatures were held at 660 and 600 °C, respectively, for 150 s in an oxygen/helium ambient at 16 Torr. Vapor-phase $CdCl_2$ annealing was also performed in a CSS configuration with source and substrate temperatures fixed at 400 °C for 10 min in an oxygen/helium ambient at 400 Torr. To complete fabrication the device was contacted with an evaporated ZnTe:Cu/Au and activated using 60 s rapid thermal processing step at T = 330 °C (Li et al., 2015).

In this work we compare the morphology and composition of the heterojunction region from a matrix of four complete devices with different thermal histories:

- Device 1: No $CdCl_2$ treatment, no RTP activation
- Device 2: $CdCl_2$ treatment, no RTP activation
- Device 3: RTP activation, no $CdCl_2$ treatment
- Device 4: Complete device with both $CdCl_2$ treatment and RTP activation

Table 1 provides representative device parameters for the 4 conditions, which were obtained by averaging several devices from fabricated from each sample. Devices 1–3 exhibited poor rectification with efficiency's < 2%, illustrating that both $CdCl_2$ and back contact activation, which provides Cu, are critical to performance as observed in

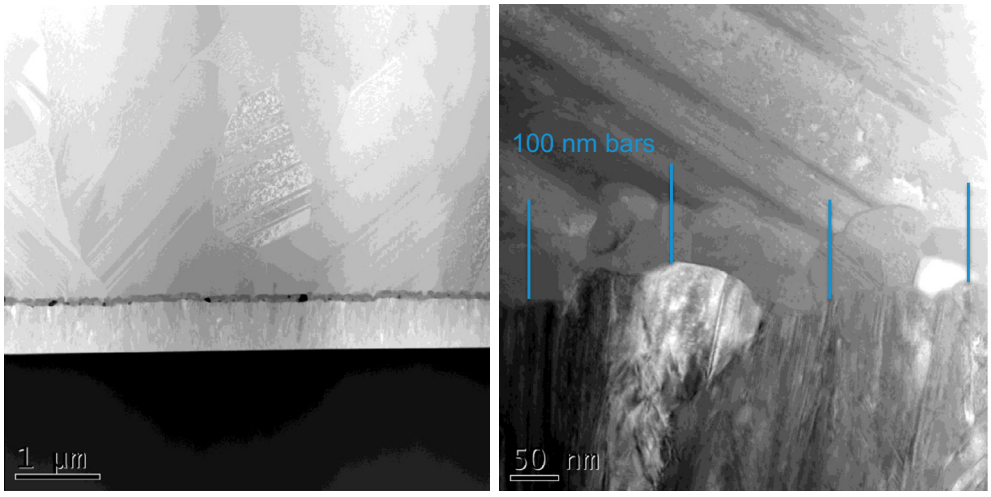

Fig. 1. TEM images of the heterojunction region of device 1 at low and high magnification showing the reduction in film thickness and evidence of polycrystalline grain morphology.

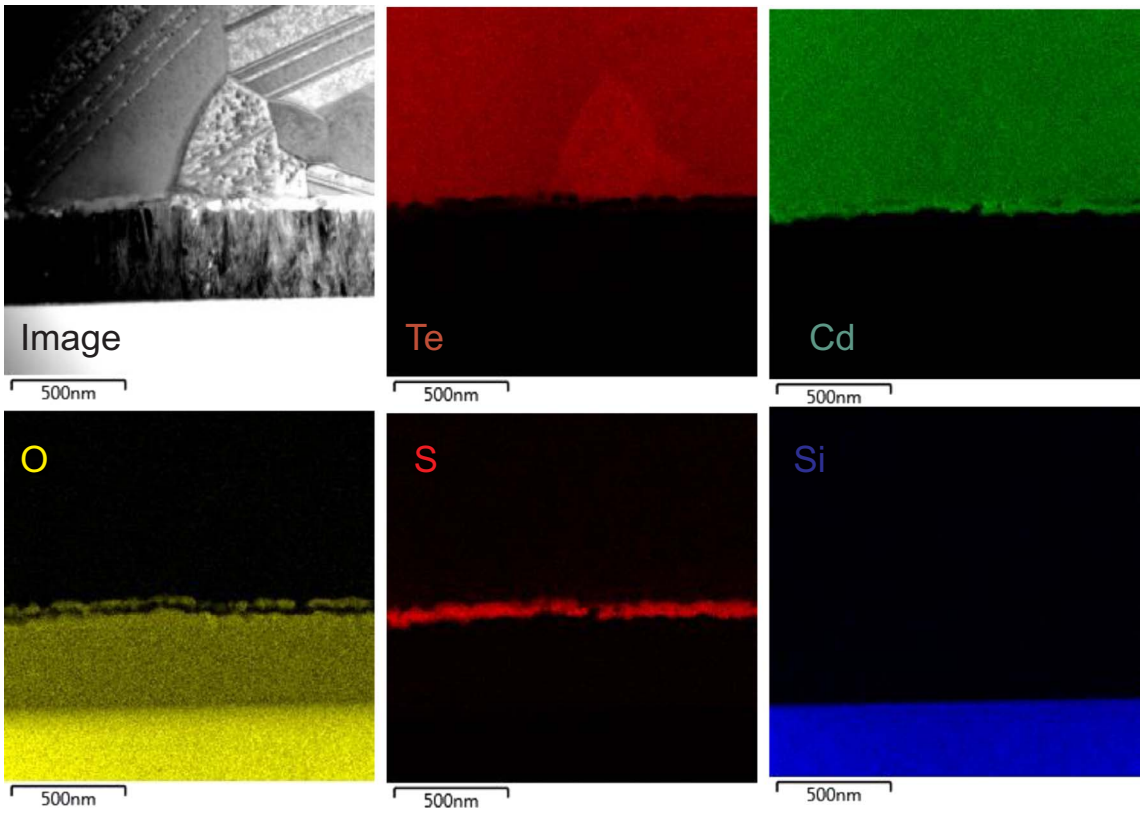

Fig. 2. Bright field TEM image and associated elemental maps from device #1 without $CdCl_2$ treatment or RTP activation.

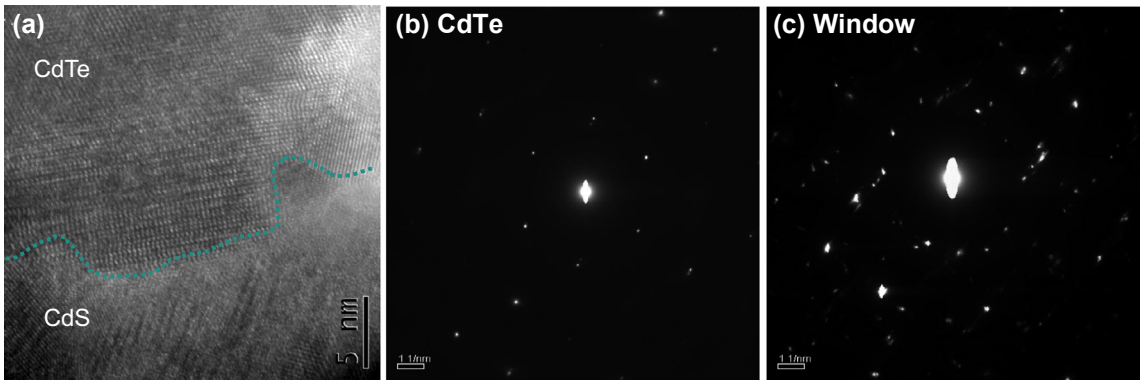

Fig. 3. (a) HR-TEM images of the interface region in device 1 showing the lattice fringes of the two crystalline phases and the abrupt transition between them. Selected area diffraction (SAD) images obtained from (b) the CdTe region and (c) the window region.

many studies (Poplawsky et al., 2014). $CdCl_2$ treatment alone results in modest improvements in J_{sc}, while RTP alone made minor improvements to the fill factor. However, there are tremendous synergies when both are applied and the fully processed devices displayed ~16% efficiency. Device 1 provides an evaluation of the changes that occur to amorphous CdS:O during CdTe deposition. Devices 2–4 were used to isolate the individual contributions of $CdCl_2$ treatment and back contact activation. TEM samples were prepared by focused ion beam (FIB) milling using a dual beam FEI Nova 600 nanolab. A standard *in situ* lift out method described previously (Abbas et al., 2014) was employed for sample preparation. HR-TEM imaging was carried out in a FEI Technai F20 equipped with an Oxford Instruments X-Max 80 silicon drift detector (SDD) energy dispersive X-ray detector (EDX). EDX was used to produce chemical distribution maps of the cells as well as line scans. The spatial resolution of the EDX measurements was ~5 nm. Due to the absence of calibration standards quantification relied on standard sensitivity factors. This was found to over-predict the density of lighter elements (O, S) that emit X-rays at low energy and as such we use EDX for relative quantification.

3. Results and discussion

3.1. Changes resulting from CdTe deposition

Fig. 1 displays a high-angle annular dark-field (HAADF) image at modest magnification and a bright field image at high resolution of the window layer region after CSS deposition of CdTe with no further thermal treatments. Examination of the HAADF image shows that the window layer is a distinct, contiguous layer. In the HAADF image the dark regions indicate areas of low density and/or the presence of low molecular weight compounds (i.e. oxygen). In the bright field image (Fig. 1b) areas of lower density appear white. The high resolution image include 100 nm vertical scale bars that are indicative of the original thickness of the as-deposited, amorphous CdS:O layer. Taking into

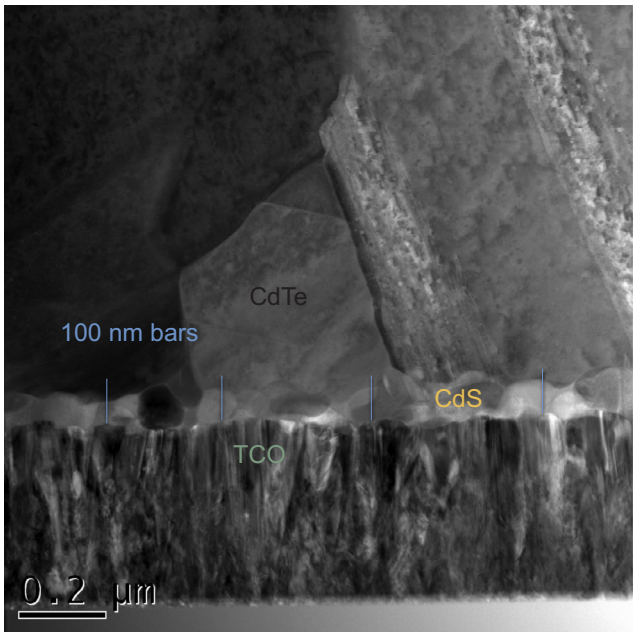

Fig. 4. Bright field TEM of the window layer from the device #2, which received $CdCl_2$ treatment but no RTP back contact activation.

account the roughness of the FTO substrate it is clear that the thickness has been reduced substantially, to around ~70 nm across the substrate. In addition, clear grains may be distinguished, indicating recrystallization during this step.

Elemental mapping was then performed to better understand the composition of the heterojunction region after CdTe deposition. Fig. 2 provides a TEM image and associated elemental maps. These images provide a qualitative measure of the composition, as the intensity was arbitrarily adjusted to maximize contrast. Perhaps the most striking map is the oxygen profile. The uniform yellow region at the bottom is the glass superstrate (see Si profile), followed by a uniform but less intense region that is the tin oxide front contact. Examination of the window layer region suggests a bilayer structure, with oxygen preferentially segregated to the interface with CdTe and diminished in the layer adjacent to the tin oxide. It is suggested that the oxygen present in the as-deposited layer is retained, but aggregates and segregates in clusters that are likely $CdSO_4$ as discussed below. The other elemental maps are consistent with this image. The sulfur signal is most intense in the region adjacent to the tin oxide. Likewise, close inspection of the Cd map reveals that its intensity is reduced immediately adjacent to the CdTe before becoming more intense adjacent to the tin oxide. Though difficult to resolve, similar features are observed in the Te map.

Fig. 3 provides a high resolution TEM of the interface between the window layer and CdTe as well as selected area diffraction (SAD) patterns obtained from the CdTe region and the window the layer, respectively. The TEM image shows that the interface is abrupt and well defined. The presence of clear lattice fringes in this image and selected area diffraction further confirm recrystallization of the window layer. The SAD pattern obtained from the CdTe region (Fig. 2b) shows the periodic array of distinct spots expected for the zinc blende crystal structure of CdTe. The SAD pattern obtained from the window region (Fig. 2c) is substantially more complicated, and it is difficult to unambiguously the crystalline phase(s) present. However, it is clearly distinct from the CdTe region, and the presence of distinct spots coupled with the absence of rings indicates that this layer consists of well-defined crystals as opposed to amorphous or highly nanocrystalline material. Aspects of the second pattern are not inconsistent with the hexagonal wurtzite structure expected for CdS and related alloys. A distinct $CdSO_4$ phase, if present, is difficult to identify as reference patterns are only available for this compound in its various hydrate forms (i.e. $CdSO_4$: H_2O_x).

To summarize, dramatic changes to the window layer occur during

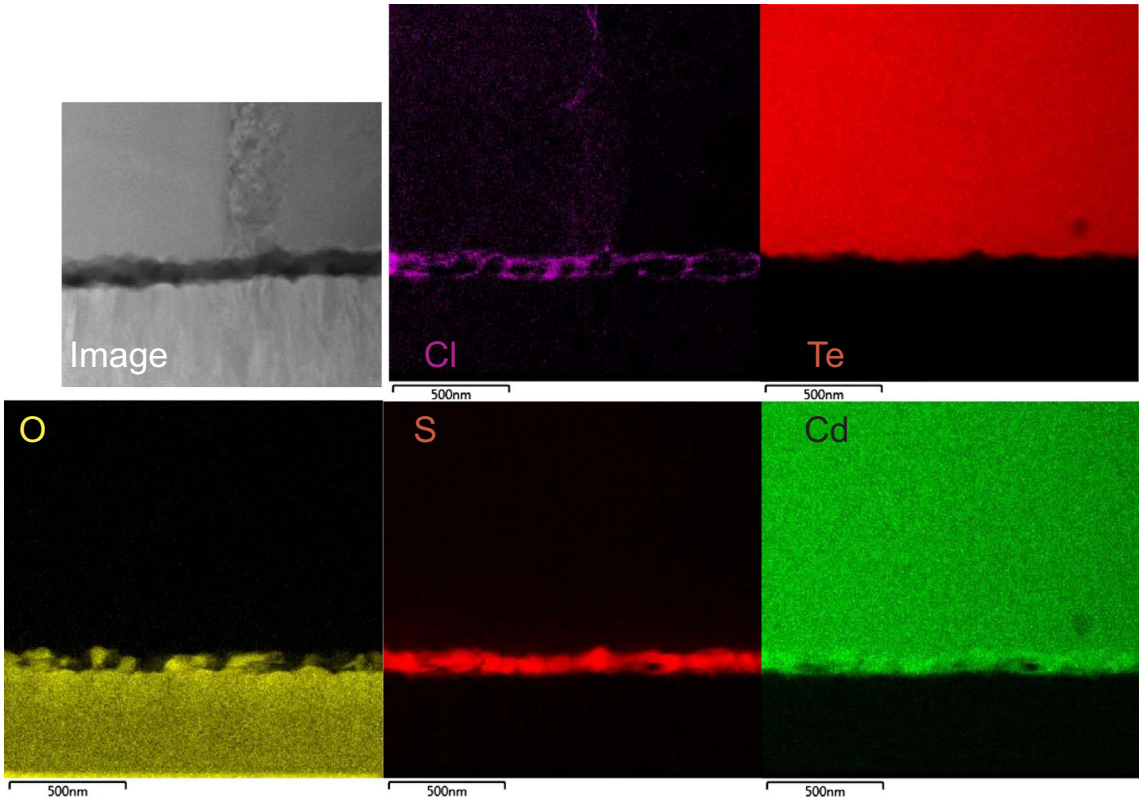

Fig. 5. HAADF TEM image and elemental mapping of the window layer from the Device #2 that received $CdCl_2$ treatment but no RTP activation.

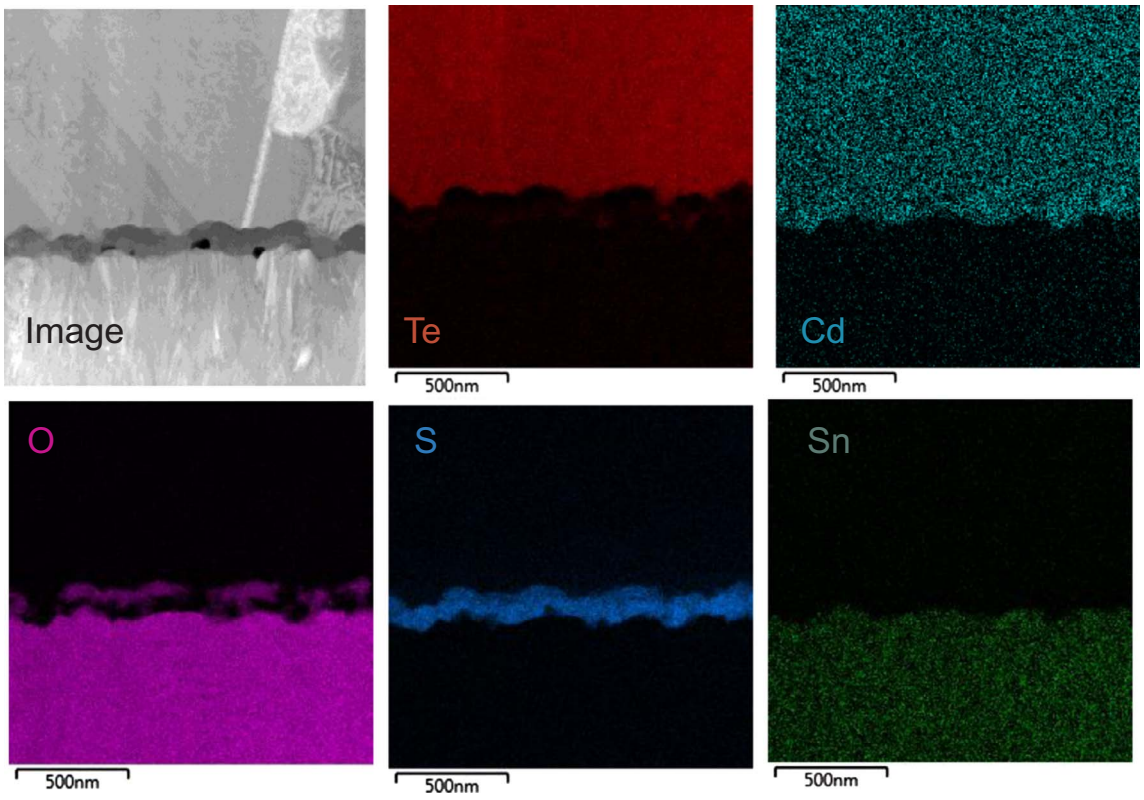

Fig. 6. HAADF TEM image and associated elemental maps from device #3 that received RTP activation but no $CdCl_2$ treatment.

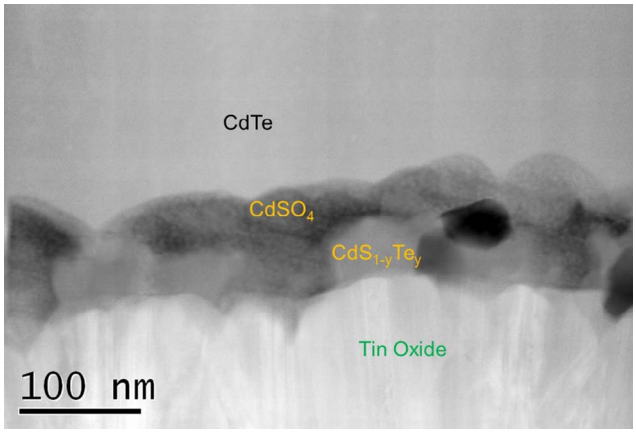

Fig. 7. High resolution image of the window layer from Device #3 with RTP activation but no $CdCl_2$ treatment.

the 2.5 min deposition of CdTe at 600 °C. The amorphous CdS:O structure is transformed into a crystalline layer whose thickness is reduced ~30% from its initial 100 nm. During CdTe deposition a bilayer structure forms consisting of a $CdSO_4$ adjacent to the CdTe and a $CdS_{1-y}Te_y$ alloy adjacent to the tin oxide. Despite these dramatic changes the window layer remains contiguous, exhibiting abrupt interfaces with both CdTe and tin oxide.

3.2. Changes resulting from $CdCl_2$ treatment

Device 2 received the standard $CdCl_2$ treatment but no back contact activation. Fig. 4 displays a bright field TEM image of the device showing the thickness and nanocrystalline nature of the window layer. Vertical 100 nm scale bars are again added for perspective. Comparisons of Figs. 1 and 4 show that the window layer thickness is nominally unchanged by the $CdCl_2$ treatment and the abrupt structural interface with CdTe is retained.

Fig. 5 displays an HAADF TEM image and elemental mapping of the window layer from device #2. The bilayer structure observed after CdTe deposition is lost. Significant oxygen remains but is now the oxygen-rich clusters are found predominantly along the interface with tin oxide. Substantial chlorine accumulation is observed in the window layer, preferentially decorating grain boundaries and the interfaces with tin oxide and CdTe. Recent XPS profiling has shown that Cl preferentially accumulates in CdS at levels of ~1 at.% after $CdCl_2$ treatment (Williams et al., 2015), and the EDX mapping is consistent with this expectation.

3.3. Changes resulting from RTP back contact activation

Our back contact consists of a co-evaporated ZnTe:Cu buffer layer followed by a gold metallization layer. The final step of device processing is activating the contact using RTP for 30 s at a set point temperature of 330 °C (Li et al., 2015). As described previously (Wolden et al., 2016) this step induces several changes in the back contact region including substantial Cu re-distribution and extensive CdTe-ZnTe interdiffusion/alloy formation. However a goal of this low thermal budget step was to restrict the impact of this step to Cu and the back contact region, leaving the bulk of the CdTe solar cell unchanged. As documented in the micrographs below, this is indeed the case. Device #3 received RTP activation but no $CdCl_2$ activation, and the structure and composition of the heterojunction region is nominally identical to Device #1 (Figs. 1–3). Fig. 6 displays a TEM and elemental mapping of Device #3. In all respects these images look nominally identical to Device #1 which did not receive RTP activation (Fig. 3). Again a bilayer structure is observed with oxygen preferentially segregated to the CdTe interface and the $CdS_{1-y}Te_y$ alloy adjacent to the tin oxide. The structure of this bilayer is shown more clearly in the high resolution HAADF image in Fig. 7.

Lastly, Fig. 8 displays TEM imaging, elemental mapping and line scans from Device #4, which received complete device processing. To

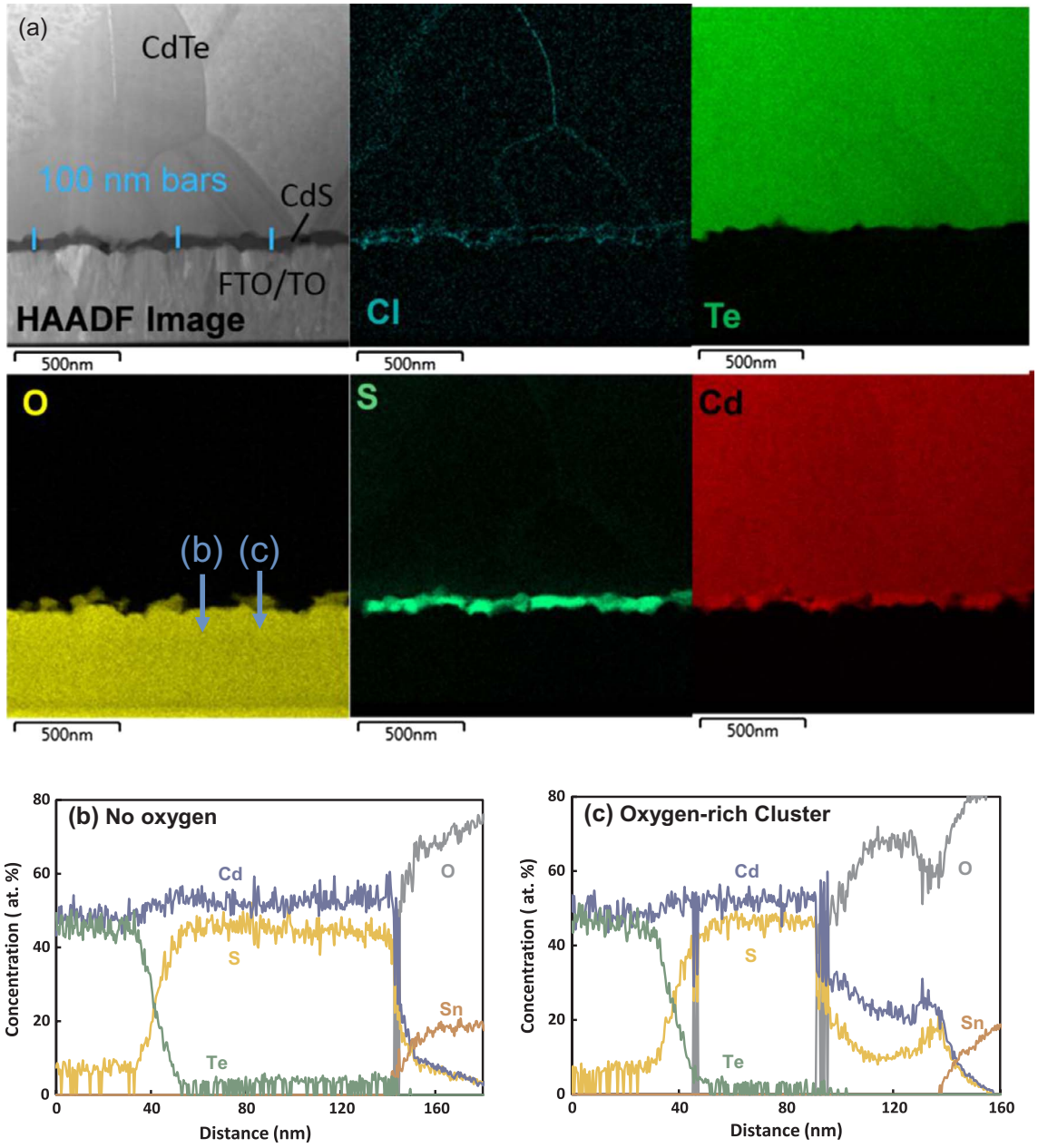

Fig. 8. (a) HR-TEM image and associated elemental maps obtained from the heterojunction region of Device #4, fully processed after both $CdCl_2$ and RTP activation. EDX line scans across window layer at positions (b) where O is not present and (c) crossing an O-rich cluster as indicated in O atom contour map.

first order Device #4 appears to be identical to Device #2, which received $CdCl_2$ treatment but no RTP activation (Figs. 4 and 5). The HAADF image shows that the window layer remains well-defined, forming rather abrupt interfaces with both tin oxide and CdTe. Comparison with the 100 nm vertical scale bars clearly shows that the thickness of the window layer varies from 50–80 nm across the sample, consistent with previous images. Chlorine is dispersed throughout the cross section, most prominently at grain boundaries in the window layer and CdTe. Decoration of these locations has been well-documented in the literature (Kranz et al., 2014; Li et al., 2014). Similar to Device #2 the bilayer structure is disrupted, with oxygen-rich clusters are found predominantly along the interface with tin oxide. The S and Cd maps confirm this, as close comparison among these three elements shows that regions of elevated O density are well correlated to regions where both the S and Cd signals are attenuated. Note that we also attempted to detect and map Cu, as migration of Cu to the front contact region has been implicated with stability issues (Wolden et al., 2016). However, no copper was detected in the front contact region of any of the four samples, indicating that if present it was well below the detection limits of EDX (~0.1 at.%)

For quantitative analysis, EDX line scans were performed across the window layer at positions with and without significant O present at the positions indicated in the O contour map (Fig. 8a). In addition to disrupting the bilayer structure, the $CdCl_2$ treatment also promotes interdiffusion between CdTe and the window layer. Across the region without oxygen present (Fig. 8b) there is a ~25 nm region characterized by strong S-Te interdiffusion as one moves out of CdTe, followed by ~80 nm of a $CdS_{1-y}Te_y$ phase where the alloy composition is essentially constant throughout until abruptly ending at the TO interface. Note that O was only detected in the tin oxide layer in this scan. The scan across the O-rich region (Fig. 8c) is initially quite similar, with a ~25 nm of Te-S interdiffusion followed by ~40 nm of a homogeneous alloy phase. However at this point a large fraction of O abruptly appears, Te falls below detection limits, and for the next 40 nm until the

TO interface the composition is characteristic of cadmium sulfate ($CdSO_4$).

The findings here are in some ways similar and some different than those reported by Klein, who used XPS to study the composition of CdS:O exposed to heat treatment but no CdTe deposition(Klein, 2015). In that study they identified signatures ascribed to CdS, $CdSO_4$, and CdO and proposed that the three phases were interspersed among each other. The significant difference here is that no regions of CdO were observed in this work. In all EDX line scans of oxygen-rich regions within the window layer both Cd and S were found to be present in significant and comparable densities, similar to what is shown in Fig. 8c. These difference in part may reflect that annealing CdS:O is not sufficient to represent the changes that occur during CdTe processing as demonstrated previously (Meysing et al., 2016). Both CdTe deposition and $CdCl_2$ treatment steps significantly impact the structure and composition of the window layer. The former leads to $CdS_{1-y}Te_y$ alloy formation and segregation of oxygen into cadmium sulfate clusters that are found along the interface with CdTe. $CdCl_2$ treatment disrupts the bilayer structure and afterwards cadmium sulfate are found to migrate towards the interface with tin oxide. While these observations are clearly documented the underlying mechanism(s) remains unclear. The presence of the ternary $CdS_{1-y}Te_y$ alloy is unsurprising since the Te fraction approaches solubility limits expected at the deposition temperature. Likewise it is postulated that $CdSO_4$ is the most thermodynamically stable state for oxygen in this reactive environment relative to alternatives such as CdO. During $CdCl_2$ treatment significant amounts of Cl migrate through the window layer to the tin oxide interface and this action may help facilitate redistribution of $CdSO_4$ clusters observed after this step. Additional work will be needed to further test and better understand these and other potential mechanisms.

4. Conclusions

The evolution of the heterojunction region in CdS:O/CdTe solar cells during device processing was systematically investigated using TEM imaging and elemental analysis. It is shown that high temperature deposition processes used for both CdTe deposition and $CdCl_2$ activation dramatically alter the structure of this region. In the first step the overall window layer thickness is reduced and a bi-layer structure is formed consisting of a nanocrystalline $CdS_{1-y}Te$ layer adjacent to the tin oxide and a cadmium sulfate region that segregates to the interface with CdTe. The $CdCl_2$ activation step does not alter the overall thickness but disrupts the bilayer structure and results in $CdSO_4$ clusters migrating towards the tin oxide interface. Chlorine preferentially segregates to the window layer, concentrated at grain boundaries and interfaces. In addition, the $CdCl_2$ treatment promotes interdiffusion with CdTe, resulting in a ~25 nm thick graded interface between the absorber and window layer. Finally it was shown that the RTP step used to activate the back contact had a negligible impact on the heterojunction region. These findings present further insight for individual process optimization.

Acknowledgements

AA and JMW were funded by UKERC through the EPSRC Supergen SuperSolar Hub. DMM, MOR, and TMB gratefully acknowledge funding from the U.S. Department of Energy through the SunShot Foundational Program to Advance Cell Efficiency (F-PACE) under Contract No. DE-AC36-08-GO28308. CAW was supported by the National Science Foundation under award CBET-1706149.

References

Abbas, A., West, G.D., Bowers, J.W., et al., 2014. Cadmium chloride assisted re-crystallization of CdTe: The effect of annealing over-treatment. In: 40th IEEE Photovoltaic Specialist Conference, pp. 0701–0706.
Green, M.A., Emery, K., Hishikawa, Y., et al., 2017. Solar cell efficiency tables (version 49). Prog. Photovolt.: Res. Appl. 25, 3–13.
Hädrich, M., Kraft, C., Metzner, H., et al., 2009. Formation of CdSxTe1–x at the p-n junction of CdS-CdTe solar cells. physica status solidi (c) 6, 1257–1260.
Kartopu, G., Clayton, A.J., Brooks, W.S.M., et al., 2014. Effect of window layer composition in $Cd_{1-x}Zn_xS$/CdTe solar cells. Prog. Photovolt.: Res. Appl. 22, 18–23.
Kephart, J.M., Geisthardt, R., Sampath, W.S., 2012. Sputtered, oxygenated CdS window layers for higher current in CdS/CdTe thin film solar cells. In: 38th IEEE Photovoltaic Specialists Conference, pp. 854–858.
Kephart, J.M., Geisthardt, R.M., Sampath, W.S., 2015. Optimization of cdte thin-film solar cell efficiency using a sputtered, oxygenated CdS window layer. Prog. Photovolt.: Res. Appl. 23, 1484–1492.
Klein, A., 2015. Energy band alignment in chalcogenide thin film solar cells from photoelectron spectroscopy. J. Phys.-Condens. Matter 27, 134201.
Kranz, L., Gretener, C., Perrenoud, J., et al., 2014. Tailoring impurity distribution in polycrystalline CdTe solar cells for enhanced minority carrier lifetime. Adv. Energy Mater. 4, 1301400.
Lane, D.W., Rogers, K.D., Painter, J.D., et al., 2000. Structural dynamics in cds–cdte thin films. Thin Solid Films 361–362, 1–8.
Li, C., Wu, Y., Poplawsky, J., et al., 2014. Grain-boundary-enhanced carrier collection in CdTe solar cells. Phys. Rev. Lett. 112, 156103.
Li, J., Diercks, D.R., Ohno, T.R., et al., 2015. Controlled activation of ZnTe: Cu contacted CdTe solar cells using rapid thermal processing. Sol. Energy Mater. Sol. Cells 133, 208–215.
Mahabaduge, H.P., Rance, W.L., Burst, J.M., et al., 2015. High-efficiency, flexible CdTe solar cells on ultra-thin glass substrates. Appl. Phys. Lett. 106, 133501.
McCandless, B.E., Engelmann, M.G., Birkmire, R.W., 2001. Interdiffusion of CdS/CdTe thin films: modeling X-ray diffraction line profiles. J. Appl. Phys. 89, 988.
McCandless, B.E., Sites, J.R., 2003. Cadmium telluride solar cells. Handbook of Photovoltaic Science and Engineering, pp. 617–662.
Meysing, D., Reese, M., Mahabaduge, H., et al., 2015. Chemical and mechanical techniques enabling direct characterization of the CdS/CdTe heterojunction region in completed devices. In: 42nd IEEE Photovoltaic Specialist Conference, pp. 1–6.
Meysing, D.M., Reese, M.O., Warren, C.W., et al., 2016. Evolution of oxygenated cadmium sulfide (CdS:O) during high-temperature CdTe solar cell fabrication. Sol. Energy Mater. Sol. Cells 157, 276–285.
Meysing, D.M., Wolden, C.A., Griffith, M.M., et al., 2015b. Properties of reactively sputtered oxygenated cadmium sulfide (CdS:O) and their impact on CdTe solar cell performance. J. Vac. Sci. Technol., A 33, 021203.
Nakamura, K., Gotoh, M., Fujihara, T., et al., 2003. Influence of CdS window layer on 2-μm thick CdS/CdTe thin film solar cells. Sol. Energy Mater. Sol. Cells 75, 185–192.
Paudel, N.R., Grice, C.R., Xiao, C., et al., 2014. The effects of high temperature processing on the structural and optical properties of oxygenated CdS window layers in CdTe solar cells. J. Appl. Phys. 116, 044506.
Paudel, N.R., Yan, Y., 2013. Fabrication and characterization of high-efficiency CdTe-based thin-film solar cells on commercial SnO_2:F-coated soda-lime glass substrates. Thin Solid Films 549, 30–35.
Poplawsky, J.D., Paudel, N.R., Li, C., et al., 2014. Direct imaging of Cl- and Cu-induced short-circuit efficiency changes in CdTe solar cells. Adv. Energy Mater. 4, 1400454.
Sites, J.R., 2003. Quantification of losses in thin-film polycrystalline solar cells. Sol. Energy Mater. Sol. Cells 75, 243–251.
Soo, Y.L., Sun, W.H., Weng, S.C., et al., 2006. Local environment surrounding S and Cd in CdS: O thin film photovoltaic materials probed by x-ray absorption fine structures. Appl. Phys. Lett. 89, 131908.
Turck, J., Nonnenmacher, H.J., Connor, P.M.L., et al., 2016. Copper (i) oxide (Cu_2O) based back contact for p-i-n CdTe solar cells. Prog. Photovolt.: Res. Appl. 24, 1229–1236.
Williams, B.L., Major, J.D., Bowen, L., et al., 2015. A comparative study of the effects of nontoxic chloride treatments on CdTe solar cell microstructure and stoichiometry. Adv. Energy Mater. 5, 1500554.
Wolden, C.A., Abbas, A., Li, J., et al., 2016. The roles of ZnTe buffer layers on CdTe solar cell performance. Sol. Energy Mater. Sol. Cells 147, 203–210.
Wu, X., Dhere, R.G., Yan, Y., et al., 2002. High-efficiency polycrystalline CdTe thin-film solar cells with an oxygenated amorphous cds (a-CdS:O) window layer. In: 29th IEEE Photovoltaic Specialists Conference, pp. 531–534.
Wu, X., Yan, Y., Dhere, R.G., et al., 2004. Nanostructured CdS:O film: preparation, properties, and application. physica status solidi (c) 1, 1062–1066.